Spatial recurrence for nonlinear magnetostatic wave excitations

Mark M. Scott,[a] Boris A. Kalinikos,[b] and Carl E. Patton
Department of Physics, Colorado State University, Fort Collins, Colorado 80523

(Received 15 May 2003; accepted 10 August 2003)

Spatial recurrence for nonlinear magnetic excitations has been observed. The recurrence was produced from the induced modulational instability of two input magnetostatic backward volume waves in a thin yttrium iron garnet film. The nominal frequency, frequency separation, and wave number were 5.5 GHz, 8 MHz, and 100 rad/cm, respectively. The spatial recurrence of the temporal wave form included frequency doubling and cnoidal profiles. A superposition of modes based on the observed Fourier makeup of the signals and calculated nonlinear phase shifts gave a response which matched the data. © *2003 American Institute of Physics.* [DOI: 10.1063/1.1615297]

I. INTRODUCTION

The concept of recurrence in nonlinear wave physics was introduced by Fermi, Pasta, and Ulam (FPU) in 1955.[1] From numerical investigations for nonlinearly coupled oscillators, they found that the energy of an initially excited monochromatic mode did not, in the long-time evolution, distribute itself among all of the accessible modes. Rather, the energy transfer involved only a few modes and gave a periodic return to the initially excited state. These results demonstrate a *spectral* recurrence, which is now called FPU recurrence. This effect has served as a catalyst for numerous investigations into nonlinear wave dynamics, including investigations into the soliton concept and modulational instability.[2,3] FPU recurrence has been observed in many physical systems, including deep water,[4] plasmas,[5] electrical networks,[3] and optical fibers.[6] In each case, the nonlinear excitations which showed FPU recurrence were obtained through a spontaneous self modulational instability (MI) process for a single monochromatic input wave.

There exists a second instability process known as *induced* MI. In contrast to the *spontaneous* instability process, the induced MI process is driven through the application of two separate input waves at different frequencies. The nonlinear interaction between these signals at a high amplitude can produce a cnoidal wave response as well as solitons. The experimental and theoretical results presented herein describe a type of spatial *phase* recurrence phenomenon for nonlinear excitations derived from an *induced* MI response.

For over a decade, there have been many fundamental studies of nonlinear wave interactions in thin low loss magnetic films. Such work includes studies on magnetostatic wave (MSW) solitons,[7–9] two-dimensional spin wave bullets,[10] and trains of MSW soliton pulses produced by feedback.[11,12] However, there have been no reports on recurrence phenomena associated with these fundamental nonlinear MSW effects. Techniques for the spatial mapping of the nonlinear wave signals[10,13] allow for the investigation of recurrence in such systems.

This article reports the observation of a recurrence phenomenon for nonlinear MSW excitations produced through the induced MI process in a magnetic film. The type of recurrence observed differs fundamentally from the aforementioned FPU recurrence. In contrast with the *spectral* FPU recurrence found for excitations produced through the spontaneous self MI process, the experimental and theoretical results presented herein reveal a type of spatial *phase* recurrence for nonlinear wave forms produced through induced modulational instability. This article further reports results on the modeling of the observed phase recurrence based on the empirical Fourier makeup of the detected signals along with interference and nonlinear phase considerations. The monochromatic wave signals for these frequency components, which were essentially constant in amplitude as a function of time and distance, could be superposed, with linear and nonlinear phase terms taken into account, to reproduce the observed recurrence response. These modeling results further support the phase recurrence interpretation of the observed phenomenon.

Sections II and III summarize the experimental procedure and present the measurement results on recurrence. Section IV presents the theoretical analysis of the results. Section V gives a brief summary of the results.

II. MAGNETIC FILM STRUCTURE AND EXPERIMENTAL PROCEDURE

The experimental arrangement consisted of a long and narrow single crystal yttrium iron garnet (YIG) thin film strip with a magnetic field parallel to the long direction of the strip. Two continuous-wave (cw) microwave signals were applied to a microstrip transducer near one end of the film. The resulting MSW propagation along the strip corresponds to the magnetostatic backward volume wave (MSBVW) configuration.[14] The spatiotemporal response was measured with a recently developed time and space resolved inductive magnetodynamic probe (IMP) system.[13] At high power, the mode beating of the two signals produces nonlinear temporal profiles with a well defined spatial recurrence. At periodic distances, the temporal signals correspond to cnoidal wave or solitonlike wave trains.

[a]Electronic mail: mscott@mrcday.com
[b]Permanent address: St. Petersburg Electrotechnical University, 197376, St. Petersburg, Russia.

 © 2003 American Institute of Physics

Downloaded 07 Nov 2003 to 129.82.140.198. Redistribution subject to AIP license or copyright, see http://ojps.aip.org/japo/japcr.jsp

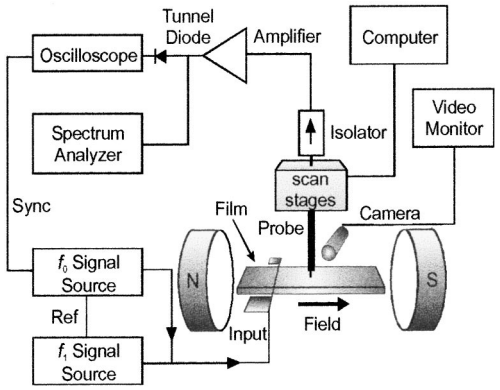

FIG. 1. Schematic diagram of the inductive magnetodynamic probe system.

Figure 1 shows a schematic diagram of the system. Phase synchronized cw signals at frequencies f_0 and f_1 are applied to an input microstrip transducer. These drive signals produce propagating MSBVW excitations within the film. The coaxial probe line is terminated with a small pick-up loop which can be scanned over the surface of the YIG film. The scan stage and detection instrumentation provide spatiotemporal data and spectral analysis for the MSBVW signals propagated in the film.

The computer controlled scan stage allows for precision positioning of the probe loop just above the film and lateral scanning of the probe over the film area with an accuracy of one μm. The spatial resolution of the probe is approximately 10 μm. The loop position is monitored through the video system. The plane of the loop was oriented perpendicular to the static field and the scan direction. For the data shown below, a 200 μm diameter probe loop was used and the loop was positioned 5 μm above the film surface. The probe was scanned along the propagation direction near the center of the YIG strip. The amplified probe signal was analyzed in two ways: (1) with a 1 ns rise time microwave tunnel diode and oscilloscope display and (2) with a microwave frequency spectrum analyzer.

The data shown below were obtained for a 6.9 μm thick single crystal YIG film with low microwave loss. The setup to observe recurrence was done in two steps. First, low power dispersion measurements with a single frequency source were made to determine an appropriate operating point. The static field was set at a nominal value of 1260 Oe to support low wave number MSBVW signal propagation in the vicinity of 5.5 GHz. The IMP system was then used with only the f_0 source operated at low power to measure the MSBVW dispersion curve of angular frequency ω versus wave number k. Theoretical fits to these data were then made, based on the Damon–Eshbach dispersion analysis. These fits were used to set the f_0 source frequency to obtain a cw response at $k \approx 130$ rad/cm. Signals with k values in this range have a strong coupling to the 50 μm wide excitation transducers and probe loop. This f_0 value was 5489 MHz.

Second, high power measurements with both sources were used to determine the working range of frequency differences for f_0 and f_1 for an induced MI response. The power of the f_0 source was increased to $P_0 = 25$ dB m. The

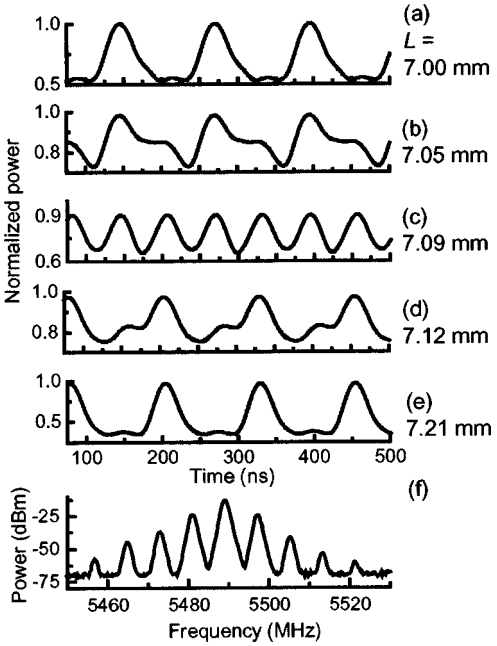

FIG. 2. Graphs (a)–(e) show profiles of detected probe power vs time for different values of the input transducer to probe spacing parameter L. Graph (f) shows the power frequency spectrum for the time trace in (a).

f_1 source was then set at 5490 MHz and a power $P_1 = 17$ dB m. This frequency was then gradually increased and the MI-induced frequency spikes in the Fourier spectrum of the detected signal were monitored. The MI spikes disappeared when f_1 was increased more than about 30 MHz above f_0.

For the recurrence data shown below, f_0 was kept at 5489 MHz and f_1 was set at 5497 MHz, well within the MI region. The f_0 and f_1 powers were kept at the values specified above. The IMP system was then used to obtain the spatiotemporal scans which provided quantitative data on recurrence.

III. RECURRENCE RESULTS FOR NONLINEAR MAGNETOSTATIC BACKWARD VOLUME WAVE EXCITATIONS

Figure 2 shows specific results for the experimental parameters given above. The graphs in Figs. 2(a)–2(e) show a sequence of average microwave power versus time traces for different values of the input transducer probe separation distance L, as indicated. The specific traces shown in Fig. 2 were selected to show one half of the spatial recurrence period. The graph in Fig. 2(f) shows a single power versus frequency spectrum which is specific to the time trace in Fig. 2(a).

First, consider the time traces. The graph in Fig. 2(a), at the $L = 7$ mm starting point selected for these particular data, shows a cnoidallike train response. As one moves down the sequence of traces for increasing L, the curves evolve. The profile in Fig. 2(e), at $L = 7.21$ mm, replicates the cnoidal form in Fig. 2(a). The middle trace in Fig. 2(c) corresponds to a temporal period doubling. As noted above, the full se-

Downloaded 07 Nov 2003 to 129.82.140.198. Redistribution subject to AIP license or copyright, see http://ojps.aip.org/japo/japcr.jsp

quence of Figs. 2(a)–2(e) shows one-half of the full recurrence period. Further traces from $L=7.21$ mm to $L=7.42$ mm would complete the cycle and show the total spatial recurrence period of 0.42 mm. It is important to emphasize that spatial recurrence is found *for all of the wave trains* shown in Fig. 2, and not just for the cnoidallike wave trains in Figs. 2(a) and 2(e). As such, the observed recurrence is *global*.

Turn now to the frequency spectrum in graph of Fig. 2(f). This spectrum, even though it was taken specifically for the time trace in Fig. 2(a), is representative of the power spectra for *all* the other time traces in Fig. 2 as well. This common power spectrum is especially significant when one considers the *completely different* temporal responses in Figs. 2(a)–2(e). This commonality, moreover, is closely tied to the global recurrence character noted above. It also provides the basis for the *phase* recurrence model employed to explain the data. This model will be considered shortly.

The power frequency spectrum in Fig. 2(f) is typical for a nonlinear response derived from the induced MI produced from two high power copropagating signals. The center peak at 5489 MHz and the next peak to the right-hand side at 5497 MHz correspond to the input signals at f_0 and f_1. Because of the high power-induced MI response, there are about seven additional peaks which fall off in intensity as one moves away from f_0 and f_1. These additional peaks are absent if the input power levels are low or if the frequency difference between f_0 and f_1 is outside the 30 MHz limit for modulational instability discussed above.

IV. RECURRENCE ANALYSIS

The common power frequency spectrum for all of the temporal signals suggests that the effect is connected with the relative phase of the component waves which make up the signal. For a given signal component at frequency ω, wave number k, and amplitude u, one may model the phase response through an equation of the form

$$k(\omega,|u|^2)=k_0+\left.\frac{\partial k}{\partial \omega}\right|_0(\omega-\omega_0)+\left.\frac{\partial^2 k}{\partial \omega^2}\right|_0(\omega-\omega_0)^2+\left.\frac{\partial k}{\partial |u|^2}\right|_0|u|^2+\ldots. \tag{1}$$

In Eq. (1), u is a scaled complex dimensionless amplitude for the wave envelope response. The usual convention is followed here, with $|u|$ proportional to $|m|/M_0$, where $|m|$ is an average dynamic magnetization amplitude and M_0 is the saturation magnetization, ω_0 and k_0 denote the carrier frequency and wave number, respectively, and the indicated derivatives are evaluated from the $k(\omega,|u|^2)$ dispersion at $|u|=0$, $\omega=\omega_0$, and $k=k_0$. Equation (1) shows the same expansion which has been used extensively with the method of envelopes to obtain the nonlinear Schrödinger equation[2,3,15] for the analysis of a wide range of problems in nonlinear wave dynamics.

From Eq. (1), one may write the response for each of the component waves which make up the total wave response. This signal response may be written in the form $A_n(x,t)=A_{n0}\cos\phi_n(x,t)$, where the phase $\phi_n(x,t)$ is given by

$$\phi_n(x,t)=\omega_n t-k(\omega_n,|u_n|^2)x=\omega_n t-\left[k_0-\frac{(\omega_n-\omega_0)}{|\nu_g|}+\frac{D}{2}\times\frac{(\omega_n-\omega_0)^2}{|\nu_g|^3}-\frac{N}{|\nu_g|}A_{n0}^2u_0^2\right]x. \tag{2}$$

In Eq. (2), the n subscripts denote the frequency component of interest. The group velocity ν_g, dispersion parameter D, and the nonlinear response parameter N correspond, respectively, to the derivative terms in Eq. (1), but with ω and k interchanged. Note that the $|u|^2$ factor in Eq. (1) is now replaced by $A_{n0}^2u_0^2$. The choice of these amplitudes and other parameters will be discussed below. By way of approximation, the phase $\phi_n(x,t)$ neglects the nonlinear cross interaction of adjacent components. The nonlinear term in Eq. (2) for the component wave labeled n contains only an $A_{n0}^2u_0^2$ amplitude term and not cross interaction terms proportional to $u_nu_{n'}$.

The above working equations were used to model the experimentally observed recurrence. The component waves defined by the nine frequency peaks in the spectrum of Fig. 2(f) were summed according to $A_{\rm sum}(x,t)=\Sigma A_{n0}\cos\phi_n(x,t)$. The A_{n0} amplitudes for the sums were scaled according to the peak heights in Fig. 2, with the biggest peak indexed at $n=0$ and normalized to $A_{00}=1$. As noted above, this peak is at the signal frequency $f_0=5489$ MHz. The common operating point frequency parameter ω_0 was set to $2\pi f_0$. Plots of $[A_{\rm sum}(x,t)]^2$ versus time were obtained for a range of x values which match as closely as possible to the experimental profiles in Figs. 2(a)–2(e).

It is to be emphasized that the component wave A_{n0} amplitudes for the sum are derived from the Fourier data in Fig. 2. The $\phi_n(x,t)$ phase factors are computed from Eq. (2). Numerical values of k_0, ν_g, and D were obtained from the low power dispersion and operating point analysis in step 1 above. These values were obtained as $k_0=130$ rad/cm, $\nu_g=3.6\times10^6$ cm/s, and $D=1300$ cm^2/rad s. The nonlinear parameter N was set to -1.1×10^{10} rad/s, based on the $|u|^2$ dependence of the MSBVW frequency in the $k\to0$ limit. The value of u_0 was estimated from an MSBVW response analysis based on Stancil[16] with the input power level set at P_0 and the other parameters as given above. This analysis gave $u_0\approx0.16$, or an average dynamic magnetization of about 16% of M_s.

Figure 3 shows a series of power versus time trace evaluations from the phase model calculation outlined above. The starting L value for the graph in Fig. 3(a) was set to give a reasonable well defined soliton train response and be close to the starting experimental L value for the graph in Fig. 1(a). The overall change in the L from Fig. 3(a) to graph Fig. 3(e) is the same as the overall change in Figs. 2(a) through 2(e) and the graph to graph incremental spacing changes are also approximately the same. The profiles in the graphs of Figs.

Downloaded 07 Nov 2003 to 129.82.140.198. Redistribution subject to AIP license or copyright, see http://ojps.aip.org/japo/japcr.jsp

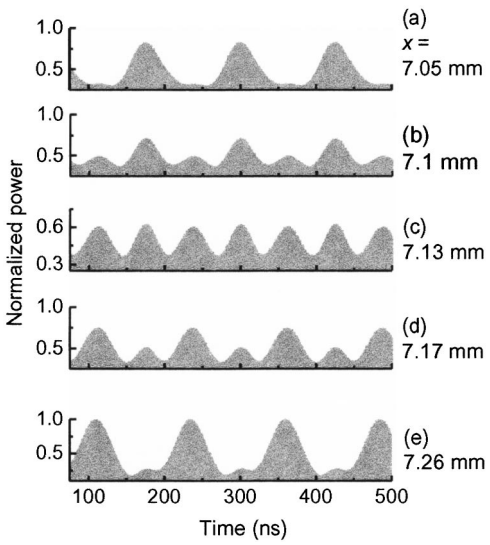

FIG. 3. Graphs (a)–(e) show traces of the calculated power vs time from the phase model for different values of the propagation distance parameter *x*, as indicated.

3(a) through 3(e) are all very close in shape to the corresponding experimental profiles in Fig. 2. These results show that simple phase model calculations reproduce all of the essential features of the Fig. 2 data. One sees the characteristic soliton train response in Figs. 3(a) and 3(e). One sees the temporal period doubling response in Fig. 3(c) and the intermediate profiles in Figs. 3(b) and 3(d). One can also see that the phase model gives the same spatial recurrence period as found experimentally.

As a final comment on the phase model calculations, it is important to note that the computed profiles are obtained with essentially one control parameter, the u_0 amplitude. All of the other parameters are obtained from experimental considerations. It is clear from Eq. (2) that the computed response will be very sensitive to the choice of $|u_0|$. In fact, no recurrent behavior of any type is observed with the model when the nonlinear parameter N is set to zero. While it may be fortuitous that a textbook calibration value of $|u_0|$ gives a nearly perfect fit to the data, the agreement nonetheless demonstrates the utility of the simple phase model to both understand and explain this fundamental nonlinear effect. Even more significant, the agreement shows that the type of nonlinearity described by the $N|u|^2$ term in Eq. (2) leads directly to the phase recurrence effect documented here. It is this same nonlinear term which is the basis of the nonlinear Schrödinger equation and most envelope soliton and MI work in the archival literature.

V. SUMMARY AND CONCLUSIONS

In summary, this work constitutes the observation of spatial recurrence for nonlinear waves obtained through induced MI. The experiment was performed through the nonlinear mode beating of two high power copropagating MSBVWs in a long and narrow magnetic film strip. The recurrence consisted of a spatially periodic evolution in the shape of the wave envelope. In spite of the evolution in the wave envelope shape, all signals shared a common power frequency spectrum. From this common spectrum, it was possible to model the recurrence in terms of a simple phase model with the same nonlinear phase shift term which is found in the nonlinear Schrödinger equation. A superposition of wave components weighted according to their measured relative amplitudes in the power frequency spectrum, in combination with a textbook calibration of the input signal response, gave good agreement with the data.

ACKNOWLEDGMENTS

This work was supported in part by the U.S. Army Research Office, Grant Nos. DAAG55-98-1-0430 and DAAD19-02-1-0197, the National Science Foundation, Grant Nos. DMR-9801649 and DMR-0108797, the North Atlantic Treaty Organization, Grant No. PST.CLG.978096, the Russian Foundation for Basic Research, Grant No. 02-02-16485, and the International Association INTAS, Grant No. 99-1812. Greg G. Boll, of GGB Industries, Inc., is acknowledged for the fabrication of the inductive probe.

[1] E. Fermi, J. Pasta, and S. Ulam, *Studies of Nonlinear Problems*, Los Alamos Scientific Laboratory Report, LA-1940 (Los Alamos, New Mexico, 1955).
[2] *Solitons*, edited by R. K. Bullough and P. J. Caudrey (Springer, New York, 1980).
[3] M. Remoissenet, *Waves Called Solitons: Concepts and Experiments* (Springer, Berlin, 1996).
[4] B. M. Lake, H. C. Yuen, H. Rungaldier, and W. E. Furgson, J. Fluid Mech. **83**, 49 (1977).
[5] *Solitons in Action*, edited by K. Lonngren and A. Scott (Academic, New York, 1978).
[6] G. V. Simaeys, P. Emplit, and M. Haelterman, Phys. Rev. Lett. **87**, 033902 (2001).
[7] V. E. Demidov, Pis'ma Zh. Eksp. Teor. Fiz. **68**, 828 (2000) [JETP Lett. **68**, 869 (1998)].
[8] H. Benner, B. A. Kalinikos, N. G. Kovshikov, and M. P. Kostylev, Pis'ma Zh. Eksp. Teor. Fiz. **72**, 306 (2000) [JETP Lett. **72**, 213 (2000)].
[9] M. M. Scott, Y. K. Fetisov, V. T. Synogach, and C. E. Patton, J. Appl. Phys. **88**, 4232 (2000).
[10] M. Bauer, O. Büttner, S. O. Demokritov, B. Hillebrands, V. Grimalsky, Y. Rapoport, and A. N. Slavin, Phys. Rev. Lett. **81**, 3769 (1998).
[11] B. A. Kalinikos, M. M. Scott, and C. E. Patton, Phys. Rev. Lett. **84**, 4697 (2000).
[12] M. M. Scott, B. A. Kalinikos, and C. E. Patton, Appl. Phys. Lett. **78**, 970 (2001).
[13] M. M. Scott, Ph.D. thesis, Department of Physics, Colorado State University, 2002.
[14] R. W. Damon and J. R. Eshbach, J. Phys. Chem. Solids **19**, 308 (1961).
[15] V. I. Karpman, *Nonlinear Waves in Dispersive Media* (Pergamon, New York, 1973).
[16] D. Stancil, *Theory of Magnetostatic Waves* (Springer, New York, 1993).

Downloaded 07 Nov 2003 to 129.82.140.198. Redistribution subject to AIP license or copyright, see http://ojps.aip.org/japo/japcr.jsp